

The finite range simple effective interaction including tensor terms

P. Bano[⊕]

School of Physics, Sambalpur University, Jyotivihar-768 019, India.

X. Viñas[‡]

Departament de Física Quàntica i Astrofísica and Institut de Ciències del Cosmos (ICCUB), Facultat de Física, Universitat de Barcelona, Martí i Franquès 1, E-08028 Barcelona, Spain

T. R. Routray[†]

School of Physics, Sambalpur University, Jyotivihar-768 019, India.

M. Centelles^{||}

Departament de Física Quàntica i Astrofísica and Institut de Ciències del Cosmos (ICCUB), Facultat de Física, Universitat de Barcelona, Martí i Franquès 1, E-08028 Barcelona, Spain

M. Anguiano[§]

Departamento de Física Atómica, Molecular y Nuclear, Universidad de Granada, E-18071 Granada, Spain

L. M. Robledo^{*}

Universidad Autónoma de Madrid, E-28049 Madrid, Spain.
Center for Computational Simulation, Universidad Politécnica de Madrid, Campus de Montegancedo, Boadilla del Monte, 28660-Madrid, Spain.

E-mail: [‡]xavier@fqa.ub.edu, [†]trr1@rediffmail.com (Corresponding author),
^{||}mariocentelles@ub.edu, [§]mangu@ugr.es, ^{*}luis.robledo@uam.es,
[⊕]mailme7parveen@gmail.com

Abstract. The prediction of single particle level crossing phenomenon between $2p_{3/2}$ and $1f_{5/2}$ orbitals in Ni - and Cu -isotopic chains by the finite range simple effective interaction without requiring the tensor part is discussed. In this case the experimentally observed crossing could be studied as a function of nuclear matter incompressibility, $K(\rho_0)$. The estimated crossing for the neutron number $N=46$ could be reproduced by the equation of state corresponding to $K(\rho_0)=240$ MeV. However, the observed proton gaps between the $1h_{11/2}$ and $1g_{7/2}$ shells in Sn and Sb isotopic chain, and the neutron gaps between the $1i_{13/2}$ and $1h_{9/2}$ shells in $N=82$ isotones, as

well as the shell closure properties at $N=28$ require explicit consideration of a tensor part as the central contribution is not enough to initiate the required level splittings.

Introduction

Different characteristics features contained in the nucleon-nucleon (NN) interaction on the top of the central short-range attractive part manifest at situations to give rise to observable effects. With the progress in the facility of producing neutron-rich isotopes far from beta-stability limit, the relevance of the tensor component in the NN interaction has gained importance over the last few decades. Since long ago the signature of a tensor component contained in the nuclear force was known from the non-vanishing electric quadrupole moment in deuteron [1, 2] but its importance in the nuclear studies using Skyrme or Gogny mean-field models have been undermined over several decades for its small contribution to the bulk nuclear properties. But the theoretical interpretation of the experimental data [3, 4, 5] on the energy gaps between single particle (s.p.) levels arising from the isotopic and isotonic effects once again established the crucial relevance of the tensor force. The presence of a tensor term in the interaction is mandatory to study new phenomena related to the evolution of the spin-orbit splittings with the neutron excess in exotic neutron-rich nuclei, as it has been pointed out, for instance, in Refs. [6, 7, 8].

The crossing of the $2p_{3/2}$ and $1f_{5/2}$ proton s.p. energy levels in neutron-rich Ni isotopes and the magic character of the atomic number $Z=28$ in this isotopic chain is a subject of current interest from both, experimental and theoretical points of view [9, 10]. The dominant s.p. character of some of the low lying excited states in neutron-rich Cu isotopes, ascertained from the γ -spectroscopic studies [10], justifies the analysis of the data using mean-field model calculation. Some phenomenological effective NN forces of Skyrme and Gogny types [11, 12], as well as the microscopic calculations based on meson-exchange interactions [6], are able to describe theoretically the $1f_{5/2}$ and $2p_{3/2}$ s.p. proton levels crossing in Ni -isotopes if a tensor component is included in the NN interaction. The underlying reason is that the tensor force modifies the spin-orbit (SO) splitting of the s.p. levels, which is crucial for obtaining the experimentally observed crossing in neutron-rich Ni isotopes. Using the Skyrme interactions Sk-III and SAMi-T, this crossing in Ni -isotopes has been achieved by adding a short-range momentum dependent tensor part [11, 13]. On the other hand, Anguiano et al have obtained the aforementioned crossing at $A=74$ by performing spherical Hartree-Fock (HF) calculations in coordinate space using the D1M Gogny interaction together with a finite-range tensor contribution [12, 14, 15]. This crossing predicted by the D1M set can also be obtained in the framework of quasi-local density functional theory (QLDFT) [16, 17] by adding a short-range tensor part as the one used in Skyrme forces, as has been shown in a recent work [18]. In this reference it has also been shown that the finite range simple effective interaction (SEI) predicts the crossing of the $1f_{5/2}$

and $2p_{3/2}$ s.p. levels in *Ni*-isotopes without requiring any explicit tensor term. This fact points out the relevance of the underlying central mean-field. In the case of SEI this level crossing phenomenon can be studied as a function of nuclear matter (NM) parameter, in particular, the incompressibility $K(\rho_0)$, as will be discussed in the present work. However, there are many other phenomena discussed in Refs. [3, 6] for which explicit consideration of a tensor term together with the SEI becomes essential to obtain the experimental trend. Our main aim in this work is to enlarge the simple effective interaction model by including a tensor term, which is chosen as short-range, similar to that used with Skyrme forces [11]. The two strength parameters of the tensor term are fixed subject to the constraint that the predicted crossing of $1f_{5/2}$ and $2p_{3/2}$ proton s.p. levels in *Ni*-isotopes and the spin inversion in the ground-state of *Cu*-isotopes remain unchanged. The paper is organized as follows. In the second section we revise the basic aspects of the mean-field approach based on the SEI paying special attention to the fitting protocol of its parameters, which is somewhat different from the one used in other effective interactions of Skyrme or Gogny types. In the same section, the short-range tensor force is briefly discussed. The third section is devoted to the discussion of the results obtained in this work. First, we show the impact of the nuclear mean-field on the proton level crossing in Ni isotopes. Next, we analyze the splitting of the $1h_{11/2} - 1g_{7/2}$ s.p. proton levels along the *Sn* and *Sb* isotopic chains and the $1i_{13/2} - 1h_{9/2}$ splitting of the s.p. neutron level in isotones of $N=82$ with the SEI model including a tensor contribution. Finally, using this model, we discuss the reduction of the spin-orbit splittings of the $1f$ and $2p$ energy levels along the $N=28$ isotonic chains when the neutron-proton asymmetry increases. Finally, our conclusions are given in the last section.

Formalism

The simple effective interaction

The SEI was introduced in Ref.[19] by Behera and collaborators. It contains altogether 11-numbers of parameters in nuclear matter, namely, α , γ , b , x_0 , x_3 , t_0 , t_3 , W , B , H , and M . This interaction reads:

$$V_{eff} = t_0(1 + x_0 P_\sigma)\delta(\vec{r}) + \frac{t_3}{6}(1 + x_3 P_\sigma) \left(\frac{\rho(\vec{R})}{1 + b\rho(\vec{R})} \right)^\gamma \delta(\vec{r}) \\ + (W + B P_\sigma - H P_\tau - M P_\sigma P_\tau) f(\vec{r}) + Spin - orbitpart. \quad (1)$$

An additional parameter, namely the strength of the the spin-orbit interaction W_0 , comes into the picture in the description of finite nuclei. The protocol adopted for the parameter determination in case of SEI is somewhat different from that of adopted in case of other effective forces. The parameter combinations responsible for the momentum dependence of the mean fields in nuclear matter of different types are fixed from experimental/empirical conditions. In this context, we impose that the mean field in symmetric nuclear matter (SNM) changes sign at kinetic energy 300 MeV

[20, 21, 22, 23], the entropy in pure neutron matter (PNM) should not exceed that of SNM [24], and the effective mass splitting in spin polarized neutron matter compares to that of the Dirac-Bruckner-Hartree-Fock (DBHF) prediction [25]. The parameter combinations responsible for the density dependence of the isospin asymmetric part of the equation of state (EoS) are fixed from the standard value of the saturation properties alongwith the empirical condition that the asymmetric nucleonic contribution in β -stable charge neutral $n + p + e + \mu$ matter be maximum. The stiffness of the SNM EOS is determined by the exponent γ of the density dependent t_3 -term, which is kept as a free parameter and all values of γ for which the pressure-density relation remains within the allowed range extracted from the analysis of the heavy-ion collision data at intermediate energies [26] are allowed. The upper limit of $\gamma \approx 1$ thus obtained for the Gaussian form of SEI corresponds to the value of incompressibility $K=283$ MeV. The density dependent term is also modified with a denominator containing the parameter b , which is ascertained so as to prevent the NM to become supraluminous [27]. With the parameters determined in this way, the SEI was able to reproduce the trends of the EoS and the momentum dependence of the mean field properties in NM with similar quality as predicted by microscopic calculations [24, 28, 29, 30, 31]. For finite nuclei calculation only remains one NM parameter open, which has been taken as t_0 . This parameter together with the SO-strength W_0 are fixed by fitting the binding energies (BEs) of the magic nuclei ^{40}Ca and ^{208}Pb . In our study, finite nuclei are described through the so-called Quasi-local Density Functional Theory (QLDFT). It is a HF calculation performed starting from the quantal energy density, but with the exchange contribution localized thorough the extended Thomas-Fermi approximation of the one-body density matrix, which contains up to second order terms in the \hbar -expansion [16, 17]. The corresponding Schrodinger equation results into a set of coupled single-particle equations,

$$\left[-\nabla \cdot \frac{\hbar^2}{2m_q^*} \nabla + U_q(\vec{R}) - \vec{W}_q(\vec{R})(\nabla \times \vec{\sigma}) \right] \phi_q = \epsilon_q \phi_q, \quad (2)$$

where the subscript $q = n, p$ indicates the type of particle, m_q^* is the effective mass, U_q is the mean-field experienced by the nucleon q , \vec{W}_q is the form-factor of the spin-orbit potential and ϵ_q is the s.p. energy corresponding to the orbital ϕ_q . This set of equations, which are local in the coordinate space, can be solved in the case of spherical symmetry in a similar way to that used for Skyrme forces. The excellent agreement between the predictions for spherical nuclei obtained using the QLDFT approximation and the full HF results has been discussed in detail in Ref.[32]. Just as an example connected with our present study, we report in Table 1 the BEs of Ni -isotopes from $A=68$ to 78 computed at QLDFT level for the four EoSs of SEI, corresponding to the γ -values $\frac{1}{6}$, $\frac{1}{3}$, $\frac{1}{2}$, and $\frac{2}{3}$, alongwith the experimental values. To deal with the pairing correlations in open-shell nuclei, we use the BCS approach together with a zero-range density-dependent pairing interaction of the type proposed by Bertsch and Esbensen and whose parameters were fitted to reproduce the pairing gaps in NM predicted by the Gogny interactions (see [32, 33] for more details.) Several studies in the domain of nuclear matter under extreme conditions Ref.[24, 31, 34] as well as in finite nuclei

Table 1. *Ni* nuclei ground state energy for $A=68$ to 78 calculated for the four EoS of SEI compared with experimental value[35].

Nuclei	SEI($\gamma = \frac{1}{6}$) E[MeV]	SEI($\gamma = \frac{1}{3}$) E[MeV]	SEI($\gamma = \frac{1}{2}$) E[MeV]	SEI($\gamma = \frac{2}{3}$) E[MeV]	Expt.[35] E[MeV]
^{68}Ni	-591.60	-591.08	-590.37	-590.46	-590.407
^{70}Ni	-604.76	-604.52	-603.80	-603.82	-602.300
^{72}Ni	-616.44	-616.32	-615.73	-615.83	-613.455
^{74}Ni	-627.04	-627.03	-626.49	-626.71	-623.82
^{76}Ni	-636.64	-636.75	-636.27	-636.53	-633.156
^{78}Ni	-645.81	-645.38	-644.96	-645.27	-641.55

Ref.[25, 32, 33], have been made using EoSs of SEI corresponding to the γ -values $\frac{1}{6}$, $\frac{1}{3}$, $\frac{1}{2}$, and $\frac{2}{3}$. These EoSs for the γ -values correspond to incompressibility in SNM 207, 226, 245, and 263 MeV, respectively. In this work we will also use the SEI EoS with $\gamma=0.42$, whose parameters alongwith the saturation properties are reported below.

The spin-orbit and the tensor force

The Skyrme-type spin-orbit interaction is used whose contribution to the energy density is given by,

$$\mathcal{H}_{SO} = -\frac{W_o}{2}[\rho\nabla \cdot \mathbf{J} + \rho_n\nabla \cdot \mathbf{J}_n + \rho_p\nabla \cdot \mathbf{J}_p]. \quad (3)$$

The spin orbit densities J_q ($q = n, p$) are given by

$$\mathbf{J}_q(\mathbf{r}) = \frac{1}{4\pi r^3} \sum_i v_i^2 (2j_i + 1)[j_i(j_i + 1) - l_i(l_i + 1) - \frac{3}{4}]R_i^2(r), \quad (4)$$

where the sum index i runs over all the quantum number labeled by $i = n, l, j$, R_i is the radial part of the wave function and v_i is the BCS occupation probability of the state. The contribution to the SO potential is obtained from the variation of H_{SO} with respect to J_q , $q = n, p$, which results into

$$\mathbf{W}_q = \frac{W_o}{2} [2\nabla\rho_q + \nabla\rho_{q'}]. \quad (5)$$

In this work we enlarge SEI by adding a tensor term, which is taken as a short-range force as the one used in Skyrme interactions. We have checked previously [18] that a QLDFT calculation with the Gogny D1M force together with a short-range tensor predicts a finite nuclei description extremely close to the one obtained in full HF calculations with a finite-range tensor [12, 14, 15]. Although the contribution of the zero-range tensor force to the energy density functional has been discussed in detail in earlier literature [5, 11], we briefly summarize it here for a sake of completeness.

The short-range tensor force including triplet-even and triplet-odd terms, with strengths T and U respectively, reads:

$$\begin{aligned} V_T = & \frac{T}{2} \left\{ \left[(\sigma_1 \cdot \mathbf{k}')(\sigma_2 \cdot \mathbf{k}') - \frac{1}{3}(\sigma_1 \cdot \sigma_2)\mathbf{k}'^2 \right] \delta(\mathbf{r}_1 - \mathbf{r}_2) \right. \\ & \left. + \delta(\mathbf{r}_1 - \mathbf{r}_2) \left[(\sigma_1 \cdot \mathbf{k})(\sigma_2 \cdot \mathbf{k}) - \frac{1}{3}(\sigma_1 \cdot \sigma_2)\mathbf{k}^2 \right] \right\} \\ & + U \left\{ (\sigma_1 \cdot \mathbf{k}')\delta(\mathbf{r}_1 - \mathbf{r}_2)(\sigma_2 \cdot \mathbf{k}) - \frac{1}{3}(\sigma_1 \cdot \sigma_2)[\mathbf{k}'\delta(\mathbf{r}_1 - \mathbf{r}_2)\mathbf{k}] \right\}, \end{aligned} \quad (6)$$

where, as usual, $\mathbf{k} = (\nabla_1 - \nabla_2)/2i$ acts on the right and $\mathbf{k}' = -(\nabla_1 - \nabla_2)/2i$ on the left. In the case of Skyrme forces the tensor interactions contribute to both binding energy and spin-orbit potential owing to their dependence on the neutron and proton spin densities, J_n and J_p , respectively [5, 11]. However, in the case of the Gogny interaction the spin densities only appear in the spin-orbit energy density within the QLDFT formalism. Therefore the tensor term only modifies the spin-orbit part of the energy density. As we are using a short-range tensor interaction, the associate energy density will read [5, 11]

$$\mathcal{H}_T = \frac{1}{2}\alpha_T [\mathbf{J}_n^2 + \mathbf{J}_p^2] + \beta_T \mathbf{J}_n \mathbf{J}_p, \quad (7)$$

where the coefficients α_T and β_T are related to the tensor strengths by

$$\alpha_T = \frac{5}{12}U \quad \beta_T = \frac{5}{24}(T + U). \quad (8)$$

If the tensor term is included, the form factor of the spin-orbit potential for each type of particles (given by the variations with respect to the spin densities \mathbf{J}_n and \mathbf{J}_p) is modified and reads

$$\mathbf{W}_q = \frac{W_o}{2} \left(2\nabla\rho_q + \nabla\rho_{q'} \right) + \alpha_T \mathbf{J}_q + \beta_T \mathbf{J}_{q'} \quad (9)$$

Results and Discussion

Impact of the incompressibility on the crossing of single particle levels in neutron rich Ni isotopes

In this work we shall examine first the influence of NM incompressibility on the $1f_{5/2}$ and $2p_{3/2}$ s.p. levels crossing phenomenon predicted in *Ni*-isotopes. For this purpose we have used the 2015 parametrization of SEI, where all the parameters are the same as Table 2 of Ref.[25] except x_0 and W_0 , which are fitted to reproduce the effective mass splitting in spin polarized PNM predicted by microscopic DBHF calculations and the BE of ^{208}Pb , respectively. The corresponding values for the different SEI EoS sets used in this work are reported in Table 4 of the same reference. The proton single particle (s.p.) energies of $1f_{7/2}$, $1f_{5/2}$, $2p_{3/2}$ and $2p_{1/2}$ in *Ni*-isotopes for $N=40$ to $N=50$ have been calculated under the QLDFT formulation using the four EoSs corresponding to $\gamma = \frac{1}{6}, \frac{1}{3}, \frac{1}{2}$, and $\frac{2}{3}$ and the corresponding results are displayed in the Fig.1. The neutron s.p. energies for $2p_{1/2}$, $1g_{9/2}$, $2d_{5/2}$ and $3s_{1/2}$, are shown in the Fig.2. Under the present

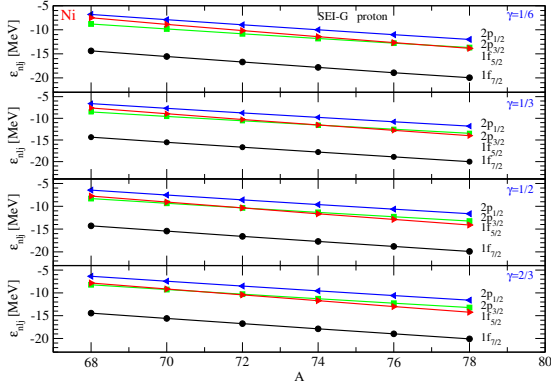


Figure 1. Proton single-particle levels around the Fermi level for Ni isotopes from $A = 68$ to $A = 78$ computed with the SEI interaction for the four EoS.

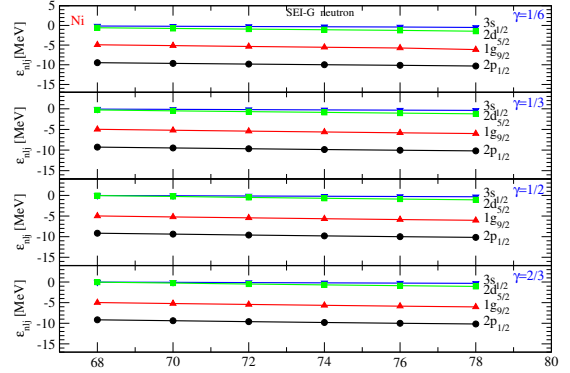


Figure 2. Neutron single-particle levels around the Fermi level for Ni isotopes from $A = 68$ to $A = 78$ computed with the SEI interaction for the four EoS.

formulation using SEI, the crossing of $1f_{5/2}$ and $2p_{3/2}$ s.p. proton levels in the isotopic chain of *Ni* is found to be a function of NM incompressibility, as can be appreciated from the results displayed in Fig.1 for the four considered EoS. As it is discussed in detail in Ref.[18], some effective forces of Skyrme and Gogny types can reproduce the crossing between the $1f_{5/2}$ and $2p_{3/2}$ proton s.p. level at mass number $A=74$, in agreement with the experimental data, only if an additional tensor force is added to these interactions. The main effect of the tensor force in the *Ni* isotopes analyzed in this work is the attraction (repulsion) between the neutron $1g_{9/2}$ s.p. level, whose occupancy grows when the mass number increases, and the $1f_{5/2}$ ($2p_{3/2}$) s.p. proton level. Notice that the presence of a tensor term does not guarantee the crossing of these s.p. proton levels, as is the case of the Skyrme-Lyon force SLy5, as has been discussed recently in [18]. This fact point out the relevance of the underlying mean-field to describe the crossing of the aforementioned s.p. proton levels. For example in the case of SEI, the crossing between the $1f_{5/2}$ and the $2d_{3/2}$ s.p. proton levels is predicted at the right mass number if a EoS with a γ -value close to $1/2$ ($K=245$ MeV) is used. SEI EoSs with smaller (larger) value of the incompressibility modulus K move the crossing point towards higher (lower) mass numbers. For instance, the EoS $\gamma = \frac{1}{6}$ ($K=207$ MeV), predicts the crossing at $A=78$ while a SEI EoS with γ -value between $1/2$ ($K=245$ MeV) and $2/3$ ($K=263$ MeV) at $A=72$.

From Fig.1 we can also see that the energy gap between the $1f_{5/2}$ and $1f_{7/2}$ proton-shells remains nearly stationary for all the four EoSs of SEI. As one moves from ^{68}Ni to ^{78}Ni , the proton energy gap, ($1f_{5/2} - 1f_{7/2}$), decreases by 0.779 MeV, 0.744 MeV, 0.741 MeV and 0.762 MeV for the EoSs $\gamma = \frac{1}{6}$, $\frac{1}{3}$, $\frac{1}{2}$, and $\frac{2}{3}$, respectively. Thus, for all

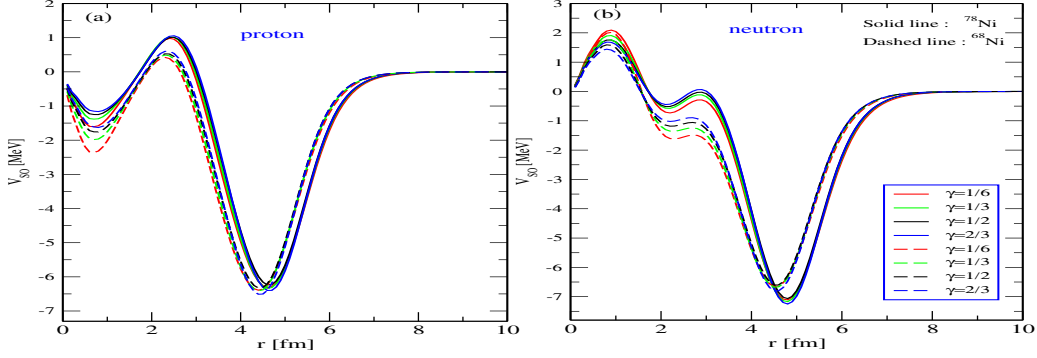


Figure 3. Proton and neutron SO-contributions in ^{68}Ni and ^{78}Ni as a function of distance r from the center of the nucleus for the four EoS.

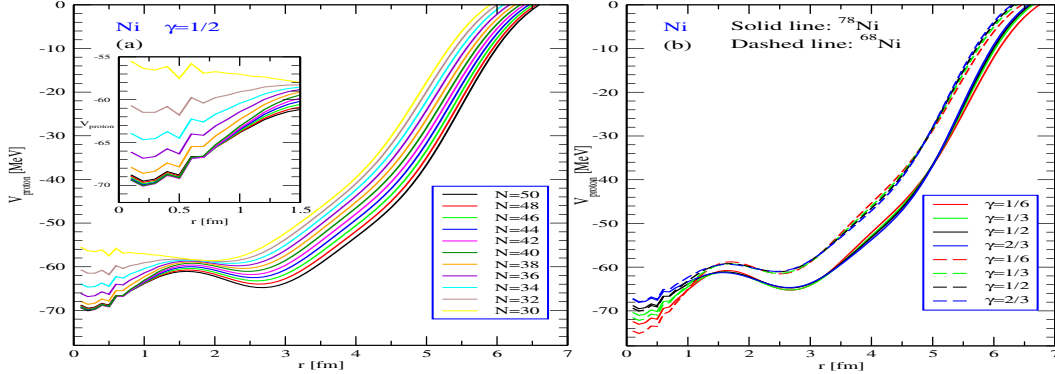


Figure 4. (a) Proton mean-field for Ni ($N=30-50$) isotopes predicted by the SEI for $\gamma = \frac{1}{2}$ under the QLDFT formulation. (b) Proton mean-field for ^{68}Ni and ^{78}Ni isotopes predicted by the SEI for $\gamma = \frac{1}{6}, \frac{1}{3}, \frac{1}{2}$ and $\frac{2}{3}$ under the QLDFT formulation.

the EoSs of SEI the magicity of $Z=28$ is preserved. The energy of the $1g_{9/2}$ and $2d_{5/2}$ s.p. neutron levels predicted by the different EoSs of SEI remain almost stationary as one moves from ^{68}Ni to ^{78}Ni , as can be seen in Fig.2. This implies that the magicity of the neutron number $N=50$ is also preserved. To get more insight about the evolution of shell structure predicted by SEI in Ni isotopes, we shall analyze the central and spin-orbit contributions to the neutron and proton mean-fields. In panels (a) and (b) of Fig.3 we display the SO contributions to p- and n- mean-fields as a function of the distance from the center for the nuclei ^{68}Ni and ^{78}Ni calculated with the four SEI EoSs used in this work. For all these four EoSs, the results are similar in quality with closely lying values. This behaviour is different from the one obtained with the D1M Gogny interaction at QLDFT level. In that case, the SO-contribution to the p-mean-

field along this Ni -isotopic chain shows a highly repulsive behaviour inside the nuclear volume as mass number increases, which is damped by the inclusion of the tensor part to the interaction that, on the other hand, has a negligibly small effect on the central potential. In panel (a) of Fig.4 we display the central part of the p-mean field for the Ni -isotopes from $N=30$ to 50 as a function of the distance from the center r computed with the EoS $\gamma = \frac{1}{2}$. We find a rather collectively compact behaviour of the p-mean-field potential curves for the isotopes corresponding to the filling of the $1g_{9/2}$ neutron shell. All the curves corresponding to $N=41$ to 50 starts from nearly identical value from well within the nuclear volume and varies smoothly as r increases, predicting a relatively higher attractive potentials for higher mass isotopes. Such collective behaviour is not noticed for the filling of $1f_{5/2}$ or $2p_{3/2}$ neutron shells in the Ni -isotopes in the mass range $40 \geq A \geq 30$. We have also checked that the D1M Gogny force at QLDFT level does not predict such a collective behaviour in the p-mean field potential curves for the Ni -isotopes when the neutron $1g_{9/2}$ is progressively occupied. The collective behaviour of the p-mean field in the Ni -isotopes in range $N=41$ to 50 is qualitatively the same at the surface for the four EoSs of SEI corresponding to $\gamma = \frac{1}{6}, \frac{1}{3}, \frac{1}{2}$ and $\frac{2}{3}$, however, some small differences appear in the nuclear volume, which is relatively more attractive for the EoS having lower value of incompressibility. This can be seen in panel (b) of Fig.4, where the p-mean fields for the ^{68}Ni and ^{78}Ni are displayed for the four EoSs of SEI considered in this work.

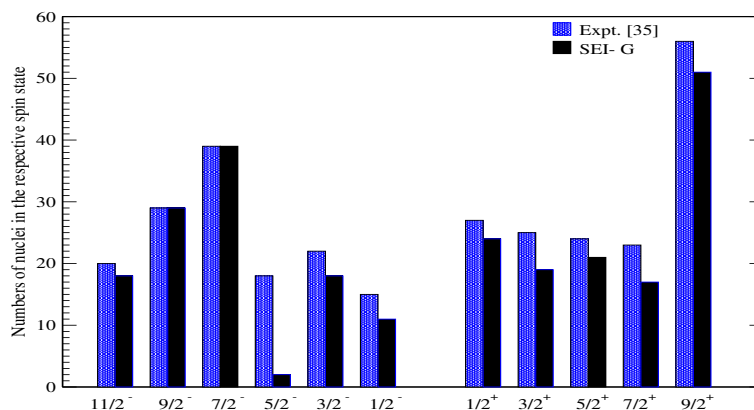


Figure 5. Comparison of experimental[35] and SEI-G($\gamma = 0.42$) spins of 298 odd-nuclei in different spin states.

The experimental data on the s.p. energy levels in Ni -isotopes are scanty and the possible information is extracted from the studies in Co , Zn , and, Cu -isotopes. In recent γ -spectroscopic studies [9, 10] of Cu -isotopes, it has been found that the inversion of the ground state spin-parity from $3/2^-$ to $5/2^-$ occurs at $N=46$. This

Table 2. Ground-state spin and energy of neutron-rich odd *Cu* isotopes predicted by the SEI EoS ($\gamma=0.42$). The energy of the first excited state E^* is also given along with the experimental results taken from Ref.[9].

Nucleus	Spin-parity	SEI($\gamma = 0.42$)	Expt.	SEI($\gamma = 0.42$)	Expt.
		Energy[MeV]	Energy[MeV]	E^* [keV]	E^* [keV]
^{69}Cu	3/2-	-599.40	-599.97	663	1215
^{71}Cu	3/2-	-613.73	-613.09	449	537
^{73}Cu	3/2-	-626.51	-625.51	156	263
^{75}Cu	5/2-	-638.25	-637.13	103	62
^{77}Cu	5/2-	-649.11	-647.42	292	295
^{79}Cu	5/2-	-658.94	-656.65	620	660

finding suggests the crossing of $2p_{3/2}$ and $1f_{5/2}$ proton s.p. levels in the underlying *Ni*-core. In order to study these *Cu* isotopes, we show first that spherical odd nuclei can also be described fairly well using SEI at QLDFE level with the uniform blocking method of Ref.[36]. The spin and parity of 298 spherical odd-nuclei have been computed with the EOS of SEI of $\gamma=0.42$ (see below), and the results are displayed in Figure 5. More than 80% of the experimental data of spin-parity of the ground-state of the odd-nuclei considered are predicted. This result is similar to the compilation of spins performed in Ref.[37] based on the results provided by several Skyrme forces and the FRDM of Möller. To investigate the inversion of the spin-parity in *Cu* isotopes, we have calculated the energy of the ground and several s.p. excited states of *Cu*-isotopes in the mass number region $A=69-79$ assuming spherical symmetry for all the considered nuclei because the deformation in these neutron-rich *Cu*-isotopes is small [38]. The ground state energies and spin-parity of the *Cu*-isotopes together with their first excited state energies are collected in Table 2 for the EoS $\gamma=0.42$.

The inversion of the ground-state spin-parity from $3/2^-$ to $5/2^-$ in *Cu* isotopes moves to smaller mass numbers when the incompressibility modulus of the SEI EoS increases. To get the right inversion point, we have varied the $K(\rho_0)$ value of the EoS by varying the exponent γ , and it has been found that for $\gamma=0.42$ the inversion of the spin-parity of the ground state occurs at $N=46$, in agreement with the experimental results [9, 10], as it can be seen in Table 2. This EoS also predicts reasonably well the energy of the first excited state, as can also be seen in the same Table 2. The calculated energies of the first excited states in other *Cu*-isotopes in this chain also compares well with the experimental results taken from Fig.2 of Ref.[9]. For example, the nucleus ^{75}Cu described by this EoS of SEI predicts the energy of excited state $3/2^-$ at 103 KeV, whereas, the experimental value is 62 KeV. The analysis of the experimental data of ^{79}Cu also suggests another excited state $1/2^-$ 1511 keV above its ground state, while the excitation energy of this state is 1957 keV according to large shell-model calculations [9] and it is predicted to be 2254

keV by the SEI EoS ($\gamma=0.42$). This EoS of SEI with $\gamma=0.42$, which predicts the inversion of the spin-parity of the ground-state from $3/2^-$ to $5/2^-$ for the nucleus ^{75}Cu and gives a satisfactory description of excited states in Cu -isotopes, has NM incompressibility modulus of $K(\rho_0)=240$ MeV. This value also conforms to the range for $K(\rho_0) = 240 \pm 20$ MeV extracted from the compressional mode of vibration in finite nuclei [39] and the ranges obtained from allied studies of isoscalar giant monopole resonance (ISGMR) and heavy-ion collisions in finite nuclei [40, 41, 42, 43]. The parameters of this SEI

Table 3. Twelve numbers of interaction parameters for SEI-G($\gamma = 0.42$) along with the nuclear matter saturation properties (such as saturation density $\rho_0(\text{fm}^{-3})$, energy per nucleon $e(\rho_0)$ (MeV), incompressibility for symmetric nuclear matter K (MeV), effective mass m^*/m , Symmetry energy E_s (MeV), Slope of symmetry energy L (MeV) and curvature of the symmetry energy K_{sym} (MeV)).

γ	$b[\text{fm}^3]$	$\alpha[\text{fm}]$	$\varepsilon_{ex}[\text{MeV}]$
0.42	0.5050	0.7591	-95.0536
$\varepsilon_{ex}^l[\text{MeV}]$	$\varepsilon_0[\text{MeV}]$	$\varepsilon_0^l[\text{MeV}]$	$\varepsilon_\gamma[\text{MeV}]$
-63.3691	-91.6562	-53.1272	90.0035
$\varepsilon_\gamma^l[\text{MeV}]$	$t_0[\text{MeV fm}^3]$	x_0	$W_0[\text{MeV}]$
65.3966	341.2	1.7933	113.4
Nuclear matter saturation properties			
$\rho_0[\text{fm}^{-3}]$	$e(\rho_0)[\text{MeV}]$	$K[\text{MeV}]$	m^*/m
0.1584	-16.0	240	0.711
$E_s[\text{MeV}]$	$L[\text{MeV}]$	$K_{sym}[\text{MeV}]$	
35.5	76.71	-155.0	

EoS of $\gamma=0.42$ alongwith the saturation properties are given in Table 3. Very recently, measurements of charge radii R_{CH} in $Z=28$ isotopes have been made [44], which allow to perform comparisons between experimental values and theoretical predictions of the charge radii in all light mass isotopic chains from $Z=19$ to $Z=50$. The charge radii R_{CH} and the isotopic shifts $\delta \langle r^2 \rangle$ computed with the SEI EoS with $\gamma=0.42$ of Ni -isotopes from ^{58}Ni to ^{72}Ni are displayed in the two panels of Fig.6 and Fig.7 together with the experimental data [44, 45]. The SEI results are in good agreement with the experimental data extracted using the Collinear laser spectroscopy and showing a similar quality as predicted by the *ab initio* calculations using the $NNLO_{sat}$ potential [44].

The role of the incompressibility is also noticed in the study of sd level splitting in Ca isotopic chain using the SEI model. Experimental studies [47, 48] establish that the proton $2s_{1/2}$ and $1d_{3/2}$ s.p. levels inverts going from ^{40}Ca to ^{48}Ca . Theoretically this inversion has been analyzed using both non-relativistic and relativistic models [49, 50, 51]. This inversion has been assigned to the action of the tensor force, and

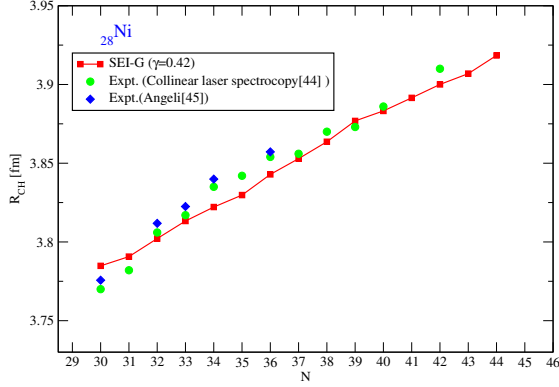


Figure 6. Nuclear charge radii R_{CH} using SEI-G ($\gamma = 0.42$) compared with the experimental data [44] and [45]).

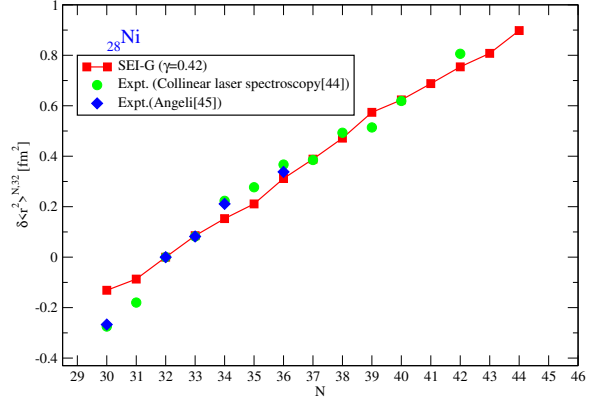


Figure 7. Isotopic shift using SEI-G ($\gamma = 0.42$) compared with the experimental data [44] and [45]).

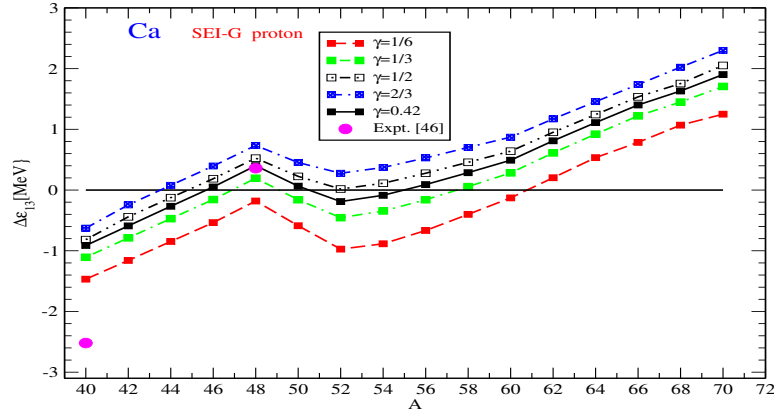


Figure 8. Energy differences of $2s_{1/2}$ and $1d_{3/2}$ proton levels ($\Delta\epsilon_{13}$) of the Ca isotopes predicted by the SEI for $\gamma = \frac{1}{6}, \frac{1}{3}, \frac{1}{2}, \frac{2}{3}$ and 0.42. The experimental data is also shown which are taken from the Ref.[46].

most of the effective interactions needs an additional tensor term to reproduce the level crossing effect. However, there are some interactions, for example, the SKI5 and SGII Skyrme forces, the D1M Gogny interaction, and the DDME1 and NL3 relativistic mean field sets, which predict the inversion of the $2s_{1/2}$ and $1d_{3/2}$ proton s.p. levels in ^{48}Ca without considering an extra tensor contribution. In Refs.[49, 50] it is found that the evolution of the orbitals and hence the energy difference $\Delta\epsilon_{13}=2s_{1/2}-1d_{3/2}$ as neutron number increases in the *Ca*-isotopic chain follows a similar trend for different interactions, irrespective of the inversion is predicted at ^{48}Ca or not. The energy difference $\Delta\epsilon_{13}$ in *Ca* isotopes is shown as a function of N in Fig.8 for the four sets of SEI,

$\gamma = \frac{1}{6}, \frac{1}{3}, \frac{1}{2},$ and $\frac{2}{3}$ together with the results for the EOS $\gamma = 0.42$. The same behaviour in the evolution of $\Delta\epsilon_{13}$ is observed in all the five sets of SEI EoSs. The gap $\Delta\epsilon_{13}$ increases from ^{40}Ca to ^{48}Ca , and then decreases to a minimum at ^{52}Ca and increases thereafter. This is a global trend observed in all the non-relativistic and relativistic interactions, as it is discussed in Refs.[49, 50]. For the SEI EoS $\gamma = 1/6$, the inversion between the $1d_{3/2}$ and $2s_{1/2}$ proton levels in ^{48}Ca , understood as a change of sign of $\Delta\epsilon_{13}$, i.e. with the $1d_{3/2}$ proton level going below of the $2s_{1/2}$ one, does not occur predicting $\Delta\epsilon_{13} = -0.18$ MeV, as it happens in case of SLy5+T interaction in Ref.[50]. For remaining four EoSs, $\gamma = \frac{1}{3}, 0.42, \frac{1}{2},$ and $\frac{2}{3}$, the inversion is predicted in ^{48}Ca , with $\Delta\epsilon_{13}$ value ranging between 195 keV to 734 keV. For the EoS $\gamma = 0.42$, $\Delta\epsilon_{13} = 401$ keV as compared to the experimental value of about 360 keV [46, 52]. On going from ^{48}Ca to ^{52}Ca , again a new inversion between the position of the $1d_{3/2}$ and $2s_{1/2}$ proton levels occurs in case of the two EoSs $\gamma = 1/3$ and 0.42, whereas for the EoSs $\gamma \geq 1/2$, although the energy gap $\Delta\epsilon_{13}$ decreases, the inversion does not take place. The occurrence of the inversion moving from ^{48}Ca to ^{52}Ca , predicted by the EoSs $\gamma = 1/3$ and 0.42, is supported with the experimental indications related to first-forbidden β -decay measurements [53]: the low-energy levels in ^{50}K are dominated by $(\pi d3/2)^{-1} (\nu d3/2)^1$ configuration which is an indication that the inversion is not present at $N = 31$ in the K chain and, thus, at $N = 32$ in the Ca chain. Beyond ^{52}Ca , $\Delta\epsilon_{13}$ increases again for all the five parameterizations of SEI. This generates another inversion with $\gamma = 1/3$ and 0.42 EoSs starting at ^{56}Ca . In this context it is to be mentioned that in the Ref.[51] it has been claimed that this inversion should occur in heavier Ca isotopes close to the two neutron drift limit, which are the predictions of the semirealistic M3Y-P5' and M3Y-P7 models based on a realistic tensor force able to reproduce the $\Delta\epsilon_{13}$ in $^{40-48}\text{Ca}$ without adjustment.

SEI plus tensor force

In the previous subsection we have discussed the crossing of $2p_{3/2}$ and $1f_{5/2}$ s.p. levels in Ni -isotopes and the inversion of the ground-state spin-parity in Cu -isotopes predicted by SEI without inclusion of a tensor term in the interaction. In this subsection we want to examine other findings those require to consider explicitly a tensor contribution to the SEI interaction eq.(1). We will analyze first the the energy differences between $1h_{11/2} - 1g_{7/2}$ proton s.p.levels in the $Z=50$ and $Z = 51$ isotopic chains and between the $1i_{13/2} - 1h_{9/2}$ s.p. neutron levels gap in the $N=82$ isotonic chain compared to the available data [3]. Next, we discuss the reduction of the spin-orbit splittings of the s.p. f and p levels at the $N=28$ closure. To this end, we compare our predictions to the experimental investigation of the $^{46}\text{Ar}(d,p)^{47}\text{Ar}$ reaction in inverse kinematics[4].

Proton gaps in the $Z=50$ and $Z = 51$ isotopic chains and neutron gaps in the $N=82$ isotonic chain: The energy gaps between the $1h_{11/2}$ and $1g_{7/2}$ proton s.p. levels and between the $1i_{13/2} - 1h_{9/2}$ s.p. neutron levels, above the $Z=50$ and $N=82$ closed shells, respectively, are investigated through QLDFT calculations using SEI in the Sn and

Sb isotopic chains and in the $N=82$ isotonic chain. The predictions of the SEI model alone in these scenarios are unable to reproduce the behaviour and the results extracted by Schiffer et al from the analysis of different experimental data that are reported in Ref. [3].

In order to get a better agreement with the results reported in [3], we add to SEI a short-range tensor term. As we have shown in Section 2, the energy density associated to the tensor force depends on the neutron and proton spin densities (see Eq.(7)), and its main effect is to modify the spin-orbit potential Eq.(9), which in turn modifies the relative position of the neutron and proton s.p. energy levels. The parameters T and U of the tensor force are chosen to describe the energy gaps given in Ref. [3] under the constraint that the crossing of $2p_{3/2}$ and $1f_{5/2}$ s.p. levels in *Ni*-isotopes at neutron number $N=46$ remains unchanged. For each pair of T and U values, the spin-orbit strength W_o is readjusted to reproduce the experimental BE of ^{208}Pb . Following this protocol we have found that for $T=800$ MeV, $U=-140$ MeV and a spin-orbit strength $W_0=122$ MeV, the f and p level crossing at $N=46$ in *Cu*- and *Ni*-isotopes remain unchanged. For higher (lower) values for T and $|U|$, the crossing shifts to higher (lower) value of N in case of *Ni*. The negative value for U is supported by the conclusion of Brown et al [54], who found that short-range tensor forces with $\alpha_T < 0$ reproduce better the experimental data in ^{132}Sn and ^{114}Sn . Our procedure of determining the tensor parameters T and U is different from the strategy used in [55], where the parameters of the tensor force are fitted to reproduce the spectra of ^{48}Ca and ^{56}Ni . We have checked that the the spin-orbit splittings of these two nuclei computed within our approach give quite similar results to the ones displayed in Figs.1 and 2 of Ref. [55].

The tensor force provides an additional attraction between neutron and proton particle or hole states with spins $j_> = l + 1/2$ and $j'_< = l' - 1/2$ (or with $j_< = l - 1/2$ and $j'_> = l' + 1/2$) and repulsion with spins $j_> = l + 1/2$ and $j'_> = l' + 1/2$ (or with $j_< = l - 1/2$ and $j'_< = l' - 1/2$). The mechanism of the tensor force, which produces the apparent attraction and repulsion between the s.p. states, is discussed in the work in Ref.[5], also applies to the theoretical results of the present work. The α_T -part of the tensor contribution to the spin-orbit form factor Eq.(9), has a constant effect without any isospin dependence. The isospin dependence enters through the β_T -part of the tensor term. As the triple-odd tensor strength U is negative, the α_T parameter is also negative. Therefore, the contribution from this term to the spin-orbit form factor is negative (positive) depending on whether \mathbf{J}_q corresponds to a $j_>$ ($j_<$) state, as can be seen from Eq.(4). The β_T -term in Eq.(9) has a positive (negative) contribution to the spin-orbit form-factor if $\mathbf{J}_{q'}$ is $j_>$ ($j_<$), as far as β_T is positive for our case. When both the contributions from α_T - and β_T -terms are negative, the spin-orbit contribution, which itself is negative, increases, thereby increasing the splitting of the s.p. states. Thus the energy gap between the $j_> = l + 1/2$ and $j'_< = l' - 1/2$ of the two different s.p. states decreases. These tensor interactions are stronger between states with similar radial wavefunctions, i.e. with the same principal quantum number and the same orbital angular momentum because in this case there is a large overlap along

the radial directions [6].

The tensor effects on the gap $1h_{11/2}-1g_{7/2}$ of the unoccupied proton states along the

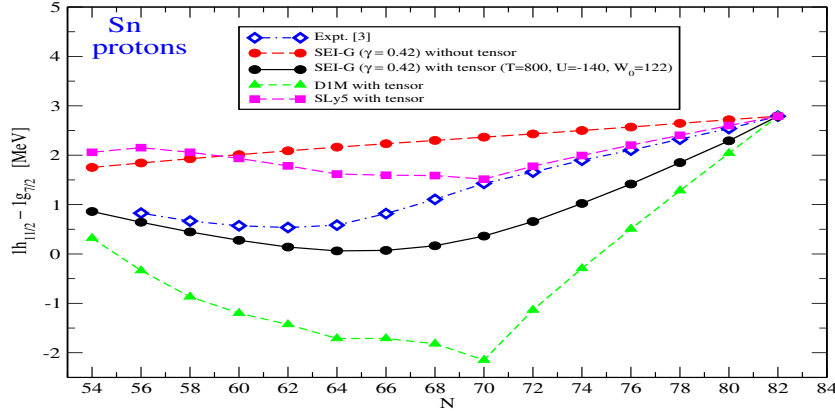


Figure 9. Energy differences between $1h_{11/2}$ and $1g_{7/2}$ proton s.p.levels in Sn -isotopes for SEI with and without Tensor. The experimental data are taken from Ref.[3]. Theoretical results have been shifted so that splittings coincide with ^{132}Sn . The corresponding results for D1M and SLy5 interaction sets with tensor are also given for comparison.

Sn -isotopic chain, shown in Fig.9, strongly depend on the position and occupancy of the neutron s.p. levels, which in the case of SEI are displayed in Figs. 10 and 11, respectively. From Fig. 10, we see that the impact of the tensor force is more important on states of large orbital angular momentum, such as $1g_{7/2}$ or $1h_{11/2}$, whose s.p. energies are clearly shifted with respect to the values computed without the tensor interaction. Above $N=50$, the neutron levels $1g_{7/2}$ and the $2d_{5/2}$ predicted by SEI lie very close to each other. The same happens with the $3s_{1/2}$ and $2d_{5/2}$ levels, while $1h_{11/2}$ remains isolate at higher s.p. energy. As can be seen from Fig. 11, from $A=100$ to $A=114$, neutrons in the Sn isotopic chain mainly populate the $1g_{7/2}$ and the $2d_{5/2}$ levels almost with the same occupation probability, which reaches at 80% at $A=114$. Above this mass number the occupancy of the $3s_{1/2}$ and $2d_{3/2}$ levels increase remarkably until about 60% in competition with the filling of the $1h_{11/2}$, which has a small occupation up to $A=120$, but from this mass number onward increases till saturate at $A=132$. The gap between the unoccupied $1h_{11/2}$ and $1g_{7/2}$ proton levels along the Sn -isotopic chain computed with and without the tensor interaction are shown in Fig.9 where we have shifted the theoretical results to coincide with the experimental value at ^{132}Sn . This gives a better insight into the evolution of the orbitals under the influence of the tensor force along the Sn -isotopic chain [56]. We have also shown the corresponding results of the D1M and SLy5 interaction sets with tensor. For SEI the shift in the cases of with and without tensor part are $\delta=2.99$ MeV and 1.85 MeV, respectively. In

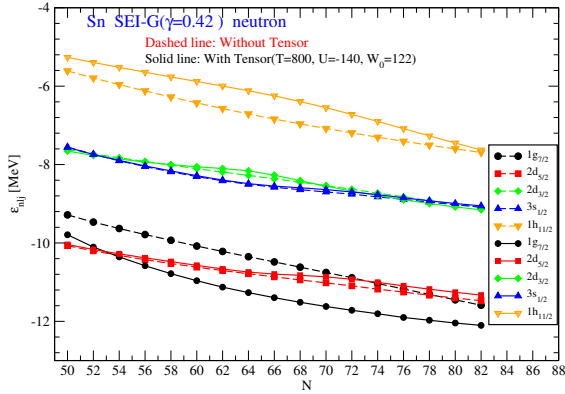


Figure 10. Neutron levels of Sn isotopes in the $N=50$ to $N=82$ major shell. Solid (dashed) lines correspond to the s.p. energies computed with (without) tensor force.

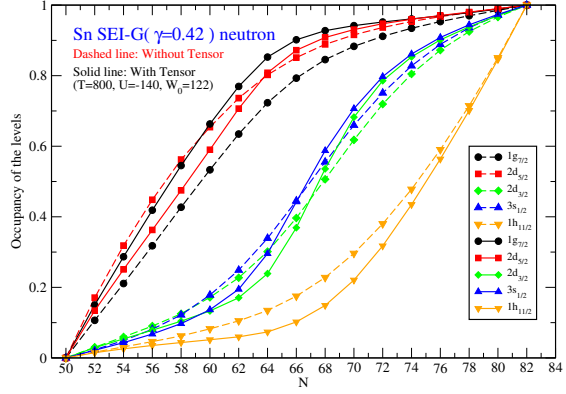


Figure 11. Occupation probability of the neutron levels of the Sn isotopes in the $N=50$ to $N=82$ major shell. Solid (dashed) lines correspond to the occupations computed with (without) tensor force.

the same figure we also show the experimental data extracted from (α, t) reaction on tin isotopes displayed in the upper panel of Fig.3 of Ref. [3]. Due to the tensor force, the filling of the $1g_{7/2}$ neutron state enhances the spin-orbit splittings of the h and g s.p. proton states, thereby decreasing the gap between the $1h_{11/2}$ and the $1g_{7/2}$ proton levels. The effect of $2d_{5/2}$ neutron level on these two proton levels is just the opposite. As the occupancy of the $1g_{7/2}$ and $2d_{5/2}$ neutron levels is quite similar, there is a partial cancellation between the tensor effects of these two neutron levels and the $1h_{11/2}$ and $1g_{7/2}$ proton levels. Due to the large overlap between the s.p wavefunction of the $1g_{7/2}$ neutron state and the $1h_{11/2}$ or $1g_{7/2}$ proton states as compared with the overlap in the case of the $2d_{5/2}$ neutron state, the SEI calculation including tensor force predicts that the $1h_{11/2}$ - $1g_{7/2}$ proton gap decreases when A increases from 100 to 114, which is in agreement with the experimental data [3]. When the mass number of the isotope increases above $A=114$, the occupancy of the $2d_{3/2}$ and $3s_{1/2}$ neutron levels becomes progressively important reaching about a 60% at $A=120$. The tensor interaction between the $2d_{3/2}$ neutron state and the $1h_{11/2}$ and $1g_{7/2}$ proton states should reduce the proton gap, however, owing to the $1h_{11/2}$ neutron level, which attracts the $1g_{7/2}$ and repels the $1h_{11/2}$ proton levels, the combined effect produces an increasing of the $1h_{11/2}$ - $1g_{7/2}$ proton gap. In spite of the small occupancy of the $1h_{11/2}$ neutron level in the range between $A=114$ and $A=120$ (see Fig. 11), the tensor interaction of this state with the $1h_{11/2}$ and $1g_{7/2}$ proton states is strong enough, due to its principal quantum number and large orbital angular momentum, to reverse the reduction of the gap due to the $2d_{3/2}$ neutron state. Finally above $A=120$, the occupancy of the $1h_{11/2}$ grows increasing the gap between the $1h_{11/2}$ and $1g_{7/2}$ proton states in agreement with the experimental

trend [3]. As it can be seen from Fig. 9, without tensor force, the SEI model predicts an almost linear smooth growing tendency with the neutron number in disagreement with the experimental results reported in [3], whose trends can be reproduced, at least qualitative, by adding the short-range tensor interaction.

We can also analyzed the $1h_{11/2}$ - $1g_{7/2}$ proton gap in the Sb isotopic chain, which behaves in a similar way as in the Sn chain discussed just before. The $1h_{11/2}$ - $1g_{7/2}$ proton gap decreases when the neutron number moves from 50 to 68, owing the progressive occupation of the $1g_{7/2}$, $2d_{5/2}$ and $1s_{1/2}$ neutron levels and increases again above $N=70$ when the occupation of the $1h_{11/2}$ neutron level grows producing a gap of ≈ 6 MeV at $N=82$. Effects due to the tensor force can be seen in the evolution of the relative separation of the unoccupied $1i_{13/2}$ - $1h_{9/2}$ neutron levels in the isotones of $N=82$ in Fig.12. Like the *Sn* isotope case we have shifted the theoretical results to coincide with the experimental value at ^{132}Sn for a better display of the influence of the tensor force along the $N=82$ isotonic chain. We have also shown the corresponding results of the D1M and SLy5 interaction sets with tensor. For SEI the shift in the cases of with and without tensor part are $\delta=1.164$ MeV and 0.904 MeV, respectively. For this isotonic chain the evolution of the proton s.p. levels in the $Z=50$ to $Z=72$ major shell and their corresponding occupancies as a function of the atomic number are displayed in Figs. 13 and 14, respectively. As proton number increases from $Z=50$ to $Z=58$, only the $1g_{7/2}$ proton level fills up until practically saturate at $Z=58$. Due to the tensor force, this proton level pulls the $1i_{13/2}$ and push the $1h_{9/2}$ neutron levels decreasing the gap between them. From $Z=58$ to $Z=64$ again only the $2d_{5/2}$ proton level fills up appreciably (see again Fig. 14), but in this case the tensor force acts in the opposite way, i.e., push up the $1i_{13/2}$ and pull down the $1h_{9/2}$ neutron levels, increasing the $1i_{13/2} - 1h_{9/2}$ neutron gap. The kink at $Z=62$ is due to the increasing of the occupancy of $2d_{3/2}$ proton level, which compensates the enlarging of the gap due to the $2d_{5/2}$ level. Beyond $Z=64$ and upto $Z=70$, the situation in the case of SEI with EOS $\gamma=0.42$ is more complicated because the $2d_{3/2}$, $3s_{1/2}$ and $1h_{11/2}$ proton levels are almost degenerated and they populate simultaneously, as it can be seen in Fig.14. In this scenario, the reduction of the $1i_{13/2} - 1h_{9/2}$ neutron gap due to the $2d_{3/2}$ proton level is compensated by the increasing effect of the $1h_{11/2}$ proton level, whose wave-function has larger overlap with the wave-functions of the neutron levels because of the same principal quantum number and similar value of the orbital angular momentum.

The SEI model plus the tensor force is also able to reproduce the experimental trends of evolution of the $1h_{11/2}$, $1g_{7/2}$ and $2d_{3/2}$ neutron s.p. levels in the $N=51$ isotonic chain. As Z increases from 40 to 50 filling the $1g_{9/2}$ proton level, the $1h_{11/2}$ neutron s.p. level is pushed up while the $1g_{7/2}$ and the $2d_{3/2}$ s.p. neutron levels are pulled down owing to the tensor interaction. The lowering of the $1g_{7/2}$ neutron level is a phenomenon pointed out by Federman and Pittel [57]. These effects are shown in Fig.15, where the evolution of these s.p. neutron levels relative to the $2d_{5/2}$ neutron level are shown for the cases of without and with tensor force. From this figure we can see that the lowering of $1g_{7/2}$ along this chain is more prominent than the one experienced by the $2d_{3/2}$ level,

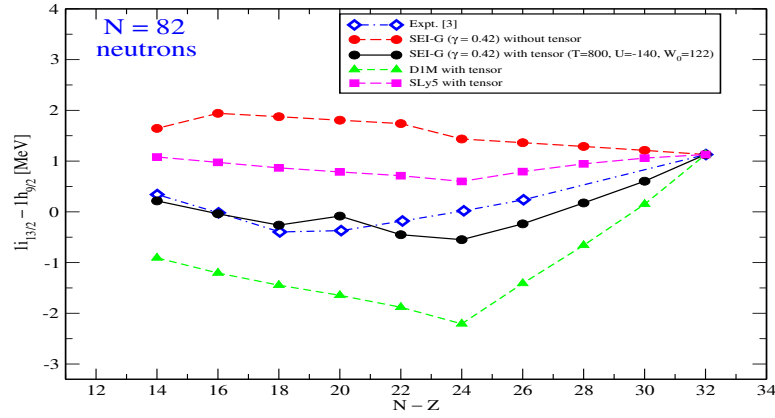


Figure 12. Energy differences between $1i_{13/2}$ and $1h_{9/2}$ neutron s.p. levels in $N = 82$ computed for SEI with and without tensor interaction. The experimental data are taken from Ref.[3]. Theoretical results have been shifted so that splittings coincide with ^{132}Sn . The corresponding results for D1M and SLy5 interaction sets with tensor are also given for comparison.

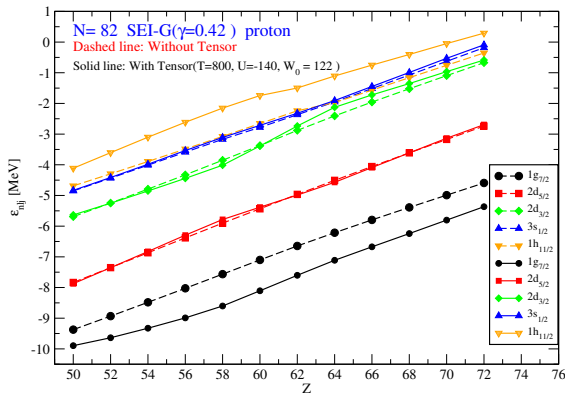


Figure 13. Proton levels of the $N=82$ isotones in the $Z=50$ - $Z=72$ major shell. Solid (dashed) lines correspond to the s.p. energies computed with (without) tensor force.

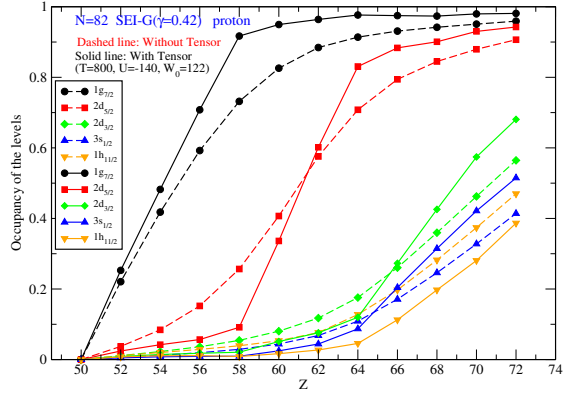


Figure 14. Occupation probability of the proton levels of the $N=82$ isotones in the $Z=50$ - $Z=72$ major shell. Solid (dashed) lines correspond to the occupations computed with (without) tensor force.

owing to the larger overlap of the wave function of the $1g_{9/2}$ proton level with the one of the $1g_{7/2}$ neutron level as compared with the overlap with the wavefunction of the $2d_{3/2}$ level.

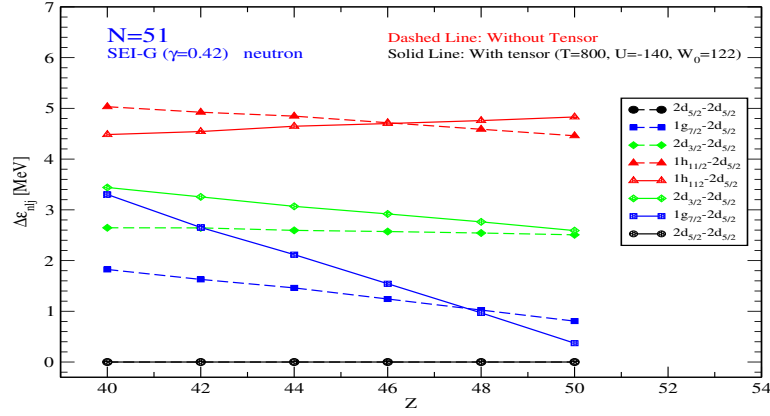


Figure 15. Neutron s.p. levels in $N=51$ isotones relative to $2d_{5/2}$ with and without Tensor.

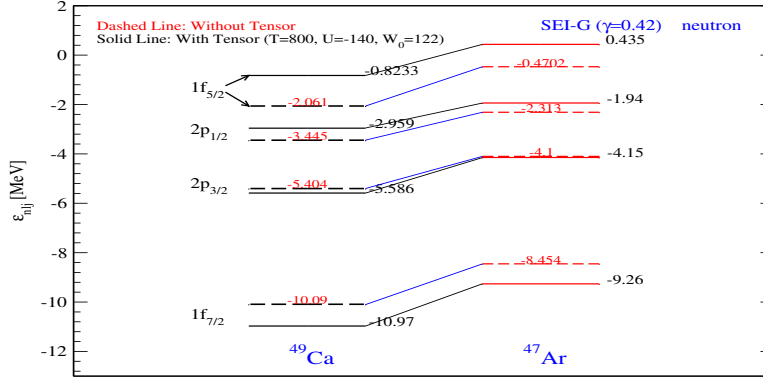


Figure 16. Neutron single-particle energies (SPE) of the fp orbitals for the $^{47}\text{Ar}_{29}$ and $^{49}\text{Ca}_{29}$ nuclei with and without Tensor

The $N=28$ gap For the nucleus ^{47}Ar , the SEI model with $\gamma=0.42$ predicts the binding energy and spin-parity of the ground-state as well as the ordering of the first excited levels, assumed of s.p. nature, in agreement with the experimental values [4]. Although this model also predicts a reduction of 332 keV of the $N=28$ gap in passing from ^{49}Ca to ^{47}Ar [4], it fails in the estimation of the reduction of the splitting of the f and p s.p. levels, which are predicted by SEI to be 45 KeV and 172 KeV, respectively, in comparison with the experimental values of 875 KeV and 890 KeV [4]. This failure can be cured, at least partially, by including a tensor component in the effective interaction. The neutron s.p. energies in the nuclei ^{49}Ca and ^{47}Ar are shown in Figure 16. We can

see that the introduction of a short-range tensor term with $T=800$ MeV and $U=-140$ MeV pulls down the $1f_{7/2}$ and $2p_{3/2}$ neutron levels and push up the $1f_{5/2}$ and $2p_{1/2}$ ones, due to the monopole effect of the interaction of neutrons with protons in the occupied level $1d_{3/2}$ [6]. As a consequence of the tensor contribution, the $N=28$ gap decreases slightly to 274 keV, but the splittings of the $1f$ and $2p$ levels in ^{47}Ar increases noticeably up to 451 and 417 KeV,

Conclusion

In this work we have used the SEI model to examine the influence of its mean-field properties, in particular the NM incompressibility $K(\rho_0)$, on the inversion of the spin-parity of the ground state observed in *Cu*-isotopes, which has a direct impact on the crossing of the $2p_{3/2}$ and $1f_{5/2}$ s.p. states in the *Ni*-isotopes. For this purpose we have considered four EoSs of the SEI family having $\gamma=\frac{1}{6}$, $\frac{1}{3}$, $\frac{1}{2}$ and $\frac{2}{3}$, which correspond to $K(\rho_0)=207$, 226, 245 and 263 MeV, respectively. The mean-field calculation have been performed within the QLDFT framework using the uniform blocking method to describe odd nuclei. This approximation is justified, as far as we have shown in a recent work [18], QLDFT and HF calculations give identical results in *Ni*-isotopic series. It is shown that in case of the SEI interaction with an incompressibility value $K(\rho_0)=240$ MeV, there is no requirement of explicit inclusion of a tensor part, unlike the case in Gogny and Skyrme forces, to achieve the $2p_{3/2}$ and $1f_{5/2}$ s.p. level crossing in *Ni*-isotopes (or the spin-parity inversion of the ground-state of *Cu*-isotopes) at the mass number $A=75$, which is the value extracted from the experiment [9, 10]. For SEI EoSs corresponding to $K(\rho_0)$ value greater than 240 MeV, the crossing of these s.p. levels occur for an isotope having $N < 46$ and vice-versa. We also show that the spin-orbit interaction in case of SEI does not turn to be highly repulsive, as observed in case of Gogny D1M case, displaying a smoothly varying behaviour as the neutron number increases from 40 to 50 along the *Ni* isotopic chain. This behaviour is different from the one exhibit by the Gogny D1M force, which shows a high repulsion at small distances. This repulsive behaviour is moderated by inclusion of a tensor force as a consequence of which the crossing of the s.p.levels in the *Ni* isotopic chain occurs at the right mass number.

We have also examined the influence of the incompressibility of the SEI EoS on the $2s_{1/2}$ and $1d_{3/2}$ proton s.p. level inversion in *Ca* isotopic chain. It is found that the EoS having $K(\rho_0)=240$ MeV ($\gamma=0.42$) reproduces the inversion effects in the *Ca* isotopic chain closely to the experimental data.

We have analyzed other scenarios where the effect of the tensor force is relevant for SEI to explain the experimental trend. To perform this study we have added to our SEI a short-range tensor interaction with two open parameters. Using SEI plus the zero-range tensor force we have studied the the gaps between the $1h_{11/2} - 1g_{7/2}$ proton s.p.levels in *Sn* isotopes and the $1i_{13/2} - 1h_{9/2}$ s.p. neutron level gaps in the $N=82$ isotonic chain comparing to the available data reported in Ref. [3]. We have also analyzed the action of the tensor force on the evolution of the $1h_{11/2}$, $1g_{7/2}$ and $2d_{3/2}$ neutron s.p. levels in the

$N=51$ isotonic chain. The tensor force produces a lowering of the $1g_{7/2}$ neutron levels when the occupancy of the $1g_{9/2}$ proton level grows, in agreement with the findings of Federman and Pittel [57]. These examples show that the SEI predictions qualitatively reproduce the experimental trends along the considered isotopic and isotonic chains, while the SEI without the tensor can not predict the experimental trend. We have also studied the variation of the $2p$ and $1f$ level splittings as well as the energy gap at $N=28$ in passing from ^{49}Ca to ^{47}Ar , for which experimental information are available [4]. We find that SEI can reproduce the gap of 330 MeV at $N=28$ but predict a small variation of the $2p$ and $1f$ splittings in passing from ^{49}Ca to ^{47}Ar . This can be cured, at least partially, by the inclusion of the tensor interaction, which in spite of a slight reduction of the energy gap at $N=28$, increases considerably the difference of the $2p$ and $1f$ splittings. In this work we see that by including a short-range tensor term to the standard spin-orbit interaction one is able to explain in a qualitative way the experimentally observed mass dependence of the specific energy gaps in Sn - and Sb -isotopes, $N=82$ and $N=51$ isotonic chains as well as the reduction in the energy gap at $N=28$ qualitatively. But to have more quantitative explanation, it appears that the tensor and the spin-orbit interactions should be modified, for example by introducing finite range in the tensor force and by exploring a more flexible spin-orbit part, which are tasks for a future research.

Acknowledgement

P.Bano acknowledges the support from MANF Fellowship of UGC, India. TRR acknowledges sincere thanks to Prof. B. Behera for meaningful discussions. M.C. and X.V. were partially supported by Grants No. FIS2017-87534-P from MINECO and No. CEX2019-000918-M from AEI-MICINN through the “Unit of Excellence María de Maeztu 2020-2023” award to ICCUB. The work of L.M.R. was partly supported by the Spanish MINECO Grant No. PGC2018-094583-B-I00. M.A has been partially supported by the Spanish MINECO Grant No. PID2019-104888GB-I00.

References

- [1] W. Rarita and J. Schwinger, Phys. Rev. **59**, 556 (1941).
- [2] J.M. Blatt and V.F.Weisskopf, Theoretical Nuclear Physics, Wiley, New York, 1952.
- [3] J P Schiffer, S J Freeman , J A Caggiano, C Deibel, A Heinz , et al., Phys. Rev. Lett. **92**, 162501 (2004).
- [4] L Gaudefroy, O Sorlin, D Beaumel, Y Blumenfeld, Z Dombra ´di, et al., Phys. Rev. Lett. **97**, 092501 (2006).
- [5] G. Colò, H. Sagawa, S. Fracasso and P.F. Bortignon, Phys. Lett. B **646**, 227 (2007).
- [6] Takaharu Otsuka, Toshio Suzuki, Rintaro Fujimoto, Hubert Grawe, and Yoshinori Akaishi, PRL **95**, 232502 (2005).
- [7] Takaharu Otsuka, Toshio Suzuki, et al., PRL **104**, 012501 (2010).
- [8] Takaharu Otsuka, Rintaro Fujimoto et al., PRL **87**, 8 (2001).
- [9] L. Olivier, S. Franchoo, M. Niikura, Z. Vajta, D. Sohler, P. Doornenbal, A. Obertelli, Y. Tsunoda, T. Otsuka, G. Authele et al., Phys. Rev. Lett. **119**, 192501 (2017).

- [10] E. Sahin, F. L. Bello Garrote, Y. Tsunoda, T. Otsuka, G. de Angelis, A. Görgen, M. Niikura, S. Nishimura, Z. Y. Xu, H. Baba et al., *Phys. Rev. Lett.* **118**, 242502 (2017).
- [11] D. M. Brink and F. Stancu, *Phys. Rev. C* **97**, 064304 (2018).
- [12] M. Anguiano, M. Grasso, G. Co', V. De Donno, and A. M. Lallena, *Phys. Rev. C* **86**, 054302 (2012).
- [13] Shihang Shen, Gianluca Colò and Xavier Roca-Maza, **99**, 034322 (2018).
- [14] M. Anguiano, A. M. Lallena, G. Co', V. De Donno, M. Grasso, and R. N. Bernard, *Eur. Phys. J. A* **52**, 183 (2016).
- [15] M. Anguiano, G. Co', V. De Donno, and A. M. Lallena, *Phys. Rev. C* **83**, 064306 (2011).
- [16] V. B. Soubotin and X. Viñas, *Nucl. Phys. A* **665**, 291 (2000).
- [17] V. B. Soubotin, V. I. Tselyaev, and X. Viñas, *Phys. Rev. C* **67**, 014324 (2003).
- [18] T. R. Routray, P. Bano , M. Anguiano, M. Centelles , X. Viñas and L. M. Robledo, *Phys. Rev C* **104**, L011302 (2021).
- [19] B Behera, T R Routray and R K Satpathy, *J. Phys. G: Nucl. Part. Phys.* **24**, 2073-2086 (1998).
- [20] G F Bertsch and S Das Gupta, *Phys. Rep.***160**, 189 (1988).
- [21] C Gale, G F Bertsch, S Das Gupta, *Phys. Rev. C* **35**, 1666 (1987).
- [22] C Gale, G M Welke, M Prakash, S J Lee, S Das Gupta, *Phys. Rev. C* **41**, 1545 (1990).
- [23] L P Csernai, G Fai, C Gale and E Osnes *Phys. Rev. C*, **46**, 736 (1992).
- [24] B Behera, T R Routray and S K Tripathy, *J. Phys. G: Nucl. Part. Phys.* **38**,115104 (2011).
- [25] B Behera, X Viñas, T R Routray and M Centelles, *J. Phys. G: Nucl. Part. Phys.* **42**, 045103 (2015).
- [26] P Danielewicz , R Lacey and W G Lynch *Science* **298**, 1592 (2002).
- [27] B Behera, T R Routray and R K Satpathy, *J. Phys G: Nucl. Part. Phys.* **23** 445 (1997).
- [28] F Sammarruca, *Int. J. Mod. Phys. E* **19** 1259 (2010).
- [29] R B Wiringa, *Phys. Rev. C* **38**, 2967 (1988).
- [30] A Akmal, V R Pandharipande and D G Ravenhall, *Phys. Rev. C* **58**, 1804 (1998).
- [31] B Behera, T R Routray and S K Tripathy, *J. Phys. G: Nucl. Part. Phys.* **36**, 125105 (2009).
- [32] B Behera, X Viñas, T R Routray, L M Robledo, M Centelles and S P Pattnaik, *J. Phys. G: Nucl. Part. Phys.* **43**, 045115 (2016).
- [33] B Behera, X Viñas, M Bhuyan, T R Routray, B K Sharma and S K Patra, *J. Phys. G: Nucl. Part. Phys.* **40**, 095105 (2013).
- [34] T R Routray, X Viñas, D N Basu, S P Pattnaik, M Centelles, L B Robledo and B Behera,*J. Phys. G: Nucl. Part. Phys.* **43**, 105101 (2016).
- [35] <https://www.nndc.bnl.gov/nudat2/>
- [36] S. Perez-Martin and L. M. Robledo, *Phys. Rev. C* **78**, 014304 (2008).
- [37] L Bonneau, P Quentin and P Möller, *Phys. Rev. C* **76** 024320 (2007).
- [38] S. Hilaire and M. Girod, The AME00 nuclear structure database, presented at the International Conference on Nuclear Data for Science and Technology, 2007, doi:10.1051/ndata:07709.
- [39] S. Shlomo, V.M. Kolomietz, and G. Colò, *Eur. Phys. J. A* **30**, 23–30 (2006).
- [40] J. R. Stone, N. J. Stone and S. A. Moszkowski, *Phys. Rev. C* **89**, 044316 (2014).
- [41] J. Piekarewicz and M. Centelles, *Phys. Rev. C* **79**, 054311 (2009).
- [42] T. Li, U. Garg, Y. Liu, R. Marks, B. K. Nayak, P. V. Madhusudhana Rao, M. Fujiwara, H. Hashimoto, K. Kawase, K. Nakanishi, S. Okumura, M. Yosoi, M. Itoh, M. Ichikawa et al, *PRL* **99**, 162503 (2007).
- [43] Yongjia Wang, Chenchen Guo, Qingfeng Li, Arnaud Le Fèvre, Yvonne Leifels, Wolfgang Trautmann, *Physics Letters B* **778**, 207–212 (2018).
- [44] S Malbrunot-Ettenauer, S Kaufmann , S Bacca, C Barbieri, J Billowes, et al., *Phys. Rev. Lett.* **128**, 022502 (2022).
- [45] I. Angeli, K.P. Marinova / *Atomic Data and Nuclear Data Tables* **99** 69–95 (2013).
- [46] H Grawe et al *Rep. Prog. Phys.* **70**, 1525 (2007).
- [47] P. Doll, G. J.Wagner, K. T. Knöpfle, and G. Mairle, *Nucl. Phys. A* **263**, 210 (1976).

- [48] C. A. Ogilvie et al., Nucl. Phys. A **465**, 445 (1987).
- [49] M. Grasso, Z. Y. Ma, E. Khan, J. Margueron, and N. Van Giai, Phys. Rev. C **76**, 044319 (2007).
- [50] Y. Z. Wang, J. Z. Gu, X. Z. Zhang, and J. M. Dong, Phys. Rev. C **84**, 044333 (2011).
- [51] H. Nakada, K. Sugiura, and J. Margueron, Phys. Rev. C **87**, 067305 (2013).
- [52] Database of the National Nuclear Data Center, Brookhaven; T. W. Burrows, Nuclear Data Sheets Update for $A = 47$. Nucl. Data Sheets **74**, 1 (1995); J. S. Hanspal et al., Nucl. Phys. A**436**, 236 (1985); S. Fortier et al., *ibid.* A**311**, 324 (1978).
- [53] P. Baumann et al., Phys. Rev. C **58**, 1970 (1998).
- [54] B.A. Brown, T. Duguet, et al., Phys. Rev. C **74** 061303(R) (2006).
- [55] Fl. Stancu, D.M. Brink, H. Flocard, Phys. Lett. B **68** 108-112 (1977).
- [56] S. Shen, G. Colò, X. Roca-Maza, EPJ Web of Conferences **223**, 01059 (2019).
- [57] P Federman and S Pittel, Phys. Lett. B **69**, 385 (1977).